data (curve 4) under the same reaction conditions. Note that the data converge at large thickness or diameter, suggesting that the calculations of the LSM surface areas, based on ideal geometry of the layers, are not significantly in error. Furthermore, the hydrogenation of ethylene ($C_2H_4 + H_2 \rightarrow C_2H_6$) on the Ni LSMs showed no thickness dependence of the specific rate, in agreement with observations made with traditional supported clusters. These results imply that only one dimension need be in the nanometer scale to produce the size effects. The LSM layer thickness is the relevant parameter. Since the surface-to-volume ratio in the LSMs is orders of magnitude smaller and the number of connected Ni atoms is orders of magnitude larger than in traditional supported catalysts, that ratio or number cannot be the source of the size effects.

The origin of the size effects must be sought in explanations that are independent of the total number of connected atoms in the metal but are dependent on the configuration of the atoms in at least one nanometer-scale dimension. Two possible explanations can be proposed, although neither can be proven at this time. One is the result of a support effect, because the metal support contact area parallel to the nanoscale dimension is essentially the same in both LSM edges and clusters. It is known that Ni and SiO_2 do not mix in the bulk, but even if that occurs on the nanometer scale in the LSMs the same effect would be present in the clusters due to similar postpreparation processing. The stoichiometry of the silica layers is not known since SiO_x may be present in the vapor-deposited layer. However, if that stoichiometric variation is the origin of the support effect, it must be present also in the cluster supports, which are prepared in a very different manner. Alternatively, the cluster and LSM surface structures could be the same. Because it is unlikely that the minimum free energy surface structure of the supported cluster matches that of the minimum free energy surface structure of the LSM edge, the LSM result suggests that neither are equilibrium structures, thus excluding those derived from the model potentials for unsupported clusters with a specific total number of atoms in them. Recent calculations of the structure of smaller unsupported clusters, made with the use of metal interaction potentials more appropriate to metals, also suggest that the surface structures in real systems could be significantly different from those previously calculated (*6*, *7*). Limited studies of supported cluster catalyst topography with tunneling microscopy further suggest that very nonideal structures are present (*8*). Although increased rates of catalytic reactions have been reported for amorphous catalysts (*9*), the larger maximum absolute rates reported here, relative to clusters, are more likely due to the narrower size distribution in the LSM edges. Finally, size-constrained surface reconstruction as a result of reaction could occur both on clusters and LSMs.

REFERENCES AND NOTES

1. M. Boudart, *Adv. Catal.* **20**, 153 (1969).
2. M. Che and C. O. Bennett, *ibid.* **36**, 55 (1989).
3. R. S. Averback, J. Bernholc, D. L. Nelson, *Clusters and Cluster-Assembled Materials*, vol. 206 of the *Materials Research Society Symposium Proceedings* (Materials Research Society, Pittsburgh, 1991).
4. I. Zuburtikudis, thesis, University of Rochester (1992).
5. T. W. Barbie, *SPIE J.* **563**, 1 (1985).
6. A. Sachdev and R. Masel, paper presented at the American Institute of Chemical Engineers 1991 Annual Meeting, Los Angeles, November 1991.
7. D. G. Vlachos, L. D. Schmidt, R. Aris, *J. Chem. Phys.* **96**, 6880 (1992).
8. P. A. Thomas, W. H. Lee, R. I. Masel, *J. Vac. Sci. Technol. A* **8**, 3653 (1990).
9. A. Molnar, G. V. Smith, M. Bartok, *Adv. Catal.* **36**, 329 (1989).
10. D. J. C. Yates, W. F. Taylor, J. H. Sinfelt, *J. Am. Chem. Soc.* **86**, 2296 (1964).
11. A. Sárkány and P. Tétényi, *React. Kinet. Catal. Lett.* **12**, 297 (1979).
12. J. H. Sinfelt, J. L. Carter, D. J. C. Yates, *J. Catal.* **24**, 283 (1972).

13. Sincere thanks to L. Fuller and D. Casilio of the Rochester Institute of Technology (Department of Microelectronics Engineering) for their decisive role in the lithography and etching work. The financial support of the Elon Huntington Hooker Fellowship to I.Z. is gratefully acknowledged.

24 June 1992; accepted 24 September 1992

Viscoelastic Dynamics of Confined Polymer Melts

Hsuan-Wei Hu and Steve Granick

The frequency-dependent shear response of an ultrathin polymer melt (polyphenylmethylsiloxane) confined between adsorbing surfaces (parallel plates of mica) is described. The sinusoidal deformations were sufficiently small to give linear response, implying that measurement did not perturb the film structure. A remarkable transition was observed with decreasing thickness. When the film thickness was less than five to six times the unperturbed radius of gyration, there emerged a strong rubber-like elasticity that was not characteristic of the bulk samples. This result indicates enhanced entanglement interactions in thin polymer films and offers a mechanism to explain the slow mobility of polymers at surfaces.

From biology to tribology, prominent interfacial processes involve polymers. With regard to surface mobility, the sharp inconsistency between theory and experiment emphasizes the prominence of some kind of trapped state in this problem (*1–3*). In this report, we are concerned with the dynamics of molten polymer of thickness comparable to the radius of gyration; other examples of unexpectedly slow surface mobility concern the spreading of polymer melts (*4*) and the adsorption-desorption dynamics of polymers in solution (*5*). Theoretical studies of the confining forces needed to maintain thin polymer films show that essentially zero force is required at equilibrium (*6*) down to a film thickness of two to three segment dimensions (*7*). Experimentally, strong repulsion is observed starting when the films are significantly thicker, several times the unperturbed radius of gyration (*8–10*). Dynamic experiments also indicate a slowing down of near-surface dynamics (*11*, *12*). However, the forced deformations in those studies caused nonlinear responses and the experiments were not designed to measure associated elastic effects. The issues raised are clearly relevant to many diverse physical phenomena, especially polymer-filler interactions in rubbers and composites (*13*), polymer adhesives, lubrication, and problems concerning the wall boundary conditions for transport during polymer processing (*14*).

We report on the linear viscoelasticity of thin polymer films. The significance of linear response (obtained with shear amplitudes <2 Å) is that measurement did not perturb the film structure. A remarkable transition was seen with diminishing film thickness. At a thickness less than five to six times the unperturbed radius of gyration (5 to 6 R_G), the viscoelastic behavior crosses from viscous relaxation, which is characteristic of single chains in the bulk liquid, to a predominantly elastic and rubber-like response. This latter response indicates enhanced steric constraints on motion, which may be construed as enhanced entanglement interactions.

The experimental approach has been reported elsewhere (*15*, *16*). In brief, the polymer fluids were confined between atomically smooth, step-free single crystals of muscovite mica that were configured as parallel plates and that were surrounded by a droplet reservoir. To measure shear

Materials Research Laboratory and Department of Materials Science and Engineering, University of Illinois, Urbana, IL 61801.

Table 1. Molecular characteristics of the PPMS samples.

Code	M_n* (g mol^{-1})	M_w/M_n†	n_n‡	R_G§ (Å)
A	2240	1.08	31	9
B	4620	1.06	65	13

*Number-average molecular weight. †Ratio of weight-average to number-average molecular weight. If all chains had the same length, this ratio would be unity. ‡Number-average number of skeletal bonds. §Unperturbed radius of gyration, estimated from the chain length by a rotational isomeric states calculation (*19*).

forces, a sinusoidal time-varying shear force was applied and the amplitude and phase of response were measured. The small influence of mechanical deformation within the device was accounted for by a model in which the calibrated properties of the device [especially the glue that attached the mica to the rest of the device (*16*)] acted in parallel with the thin film. Recent improvements have increased the system resolution and stability so that viscous forces as low as 10^{-9} N were resolved. Control experiments with shear amplitudes as low as 0.5 Å confirmed that the response was linear in amplitude over the frequencies studied, 0.03 to 250 Hz.

The polymer fluids, atactic methyl-terminated polyphenylmethylsiloxane (PPMS) (*17*), are comprised of amorphous and flexible chains that cannot crystallize because they are atactic. The bulk glass transition temperature ($T_g \approx -20$°C) (*18*) is well below the temperature of these experiments (26° ± 0.5°C), which avoids glassy dynamics complications that have been much discussed (*1*, *2*). The contact angle with mica is ~0°. Control experiments, in which PPMS was displaced from mica by water, showed that adsorption was reversible. Molecular characteristics of the samples studied are given in Table 1. The unperturbed R_G was estimated from the chain length by a rotational isomeric states calculation (*19*). The persistence length of atactic PPMS in the bulk, estimated from the characteristic ratio, is about six skeletal bonds (10 Å) (*19*). Although we have no direct measurement of the entanglement length of PPMS (because of a limited amount of sample), from the calculated chain stiffness (*19*) one expects that the molecular weight between entanglements is $M_e \approx 12{,}000$ g mol^{-1} (*20*), so that chains of the length studied here would be too short to be entangled in the bulk.

The normal pressures required to squeeze films of polymer B (65 skeletal bonds) to a specified thickness are shown in Fig. 1 (*21*). The mean normal pressure, $P_\perp$ (normal force normalized by the area of the parallel mica plates), is plotted against film thickness (D). The normal pressure rose monotonically at thickness $D < 60$ to 70 Å (5 to 6 R_G) in approximately an exponential fashion (decay length close to R_G). Because the question of equilibration is an essential point, the equilibration time for polymer A was varied by a factor of nearly 100 (20 min and 24 hours per datum) with no discernible effect.

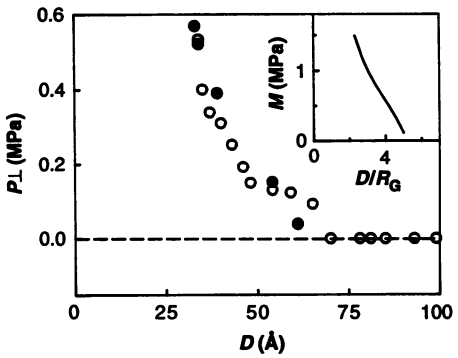

Fig. 1. Static pressure in the normal direction required to squeeze a film of polymer B (M_n = 4620 and $R_G \approx 13$ Å) to the specified separations. Open circles: equilibration time 20 min per datum. Filled circles: 24 hours per datum. Inset shows the derived bulk longitudinal modulus ratio, $M = -\delta P/\delta \ln D$, plotted against film thickness (D) normalized by R_G.

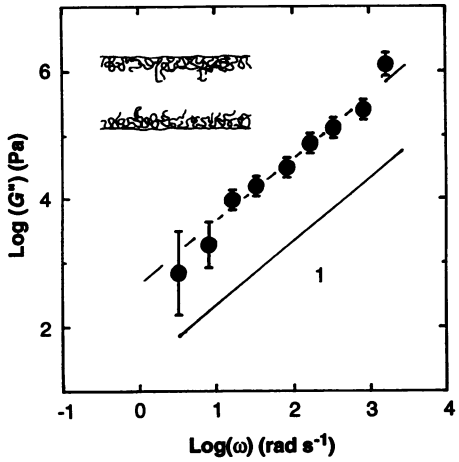

Fig. 2. Log-log plot of the loss modulus, $G''(\omega)$, as a function of angular frequency of measurement, ω, for a film of polymer A of thickness 90 ± 3 Å (7 R_G). Error bars are indicated. Inset shows a schematic illustration of the opposing solid surfaces, each carrying polymer tethered by multiple points of contact, with unattached polymer in between.

These data suggest two immediate conclusions. First, long-range repulsion in these squeezed polymer films was kinetically stable over the long time scales studied. This result decisively corroborates earlier measurements taken with shorter equilibration times (*8*–*10*). It suggests interpretation of $P_\perp(D)$ in terms of the energy to squeeze a fixed adsorbance of tethered polymer. Second, from the slope of the data in Fig. 1, the bulk longitudinal modulus [$M = -(\delta P/\delta \ln D)$] (*13*) of these molecularly thin films can be calculated. As excess polymer was squeezed out with diminishing thickness, M rose as indicated in the inset of Fig. 1. This value is used below to estimate Poisson's ratio.

Turning to the dynamic oscillatory shear forces, we consider first a film of thickness such that it did not support any normal pressure. The physical picture to imagine is an inhomogeneous system: opposing solid surfaces, each carrying polymer tethered by multiple points of contact, with unattached polymer in between. This situation is sketched schematically in the inset of Fig. 2.

In Fig. 2, $G''(\omega)$ of a film of polymer B of thickness 90 ± 3 Å (7 R_G) is plotted against radian frequency, ω, on logarithmic axes. The loss modulus, $G''(\omega)$, is the component of the oscillatory stress that (following Newton's law of viscous flow) was in phase with the rate of deformation. Here we ignore possible edge effects and assume that the length scale by which to normalize the shear amplitude is the film thickness. On physical grounds, one expects a region of polymer segments near the solid surfaces to have slower mobility, making the rheological film thickness somewhat less than the mica-mica separation (*8*–*11*). However, a correction for this effect would not change the relative values of the viscoelastic moduli, nor their orders of magnitude. Because it is not clear how to correct the raw data, we avoided such fine-tuning of the analysis.

As was expected of bulk viscous flow at low frequency, where G'' must equal $\omega\eta$ (η is the constant viscosity) (*13*), the $G''(\omega)$ data in Fig. 2 have a slope of unity. This result indicates that the inverse frequency of the experiment was larger than the longest relaxation time of the liquid. The effective viscosity [$G''(\omega)/\omega$] was $\eta_{eff} \approx 100$ Pa s. We distinguish between η_{eff} and a bulk viscosity because the structure of the system was inhomogeneous. Nonetheless, the estimate, 100 Pa s, is reasonable for the bulk response of PPMS liquid of this chain length.

The physical picture to imagine, as the polymer films were squeezed to a thickness less than 5 R_G, is a progressive interdigitation of the polymer layers that are tethered to the opposing solid surfaces.

We consider first a film thickness just at the point of onset of static forces in the normal direction. In Fig. 3, $G'(\omega)$ and $G''(\omega)$ of a film 62 ± 1 Å thick (4.8 R_G) are plotted against ω on logarithmic axes. The storage modulus, $G'(\omega)$, is the component of oscillatory stress that (following Hooke's law of elastic deformation) is in phase with the deformation. The data split into two regimes: (i) low frequencies, where $G'(\omega)$ and $G''(\omega)$ are comparable in magnitude,

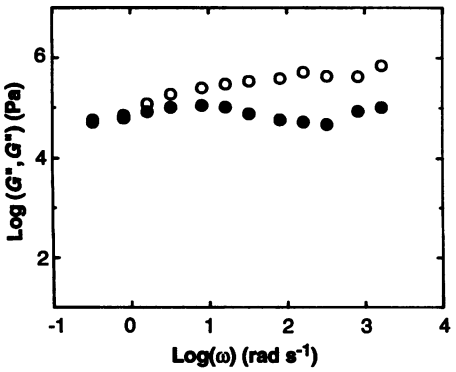

Fig. 3. Log-log plot of storage and loss shear moduli, $G'(\omega)$ and $G''(\omega)$, as a function of angular frequency of measurement, for a film of polymer B of thickness 62 ± 1 Å (4.8 R_G).

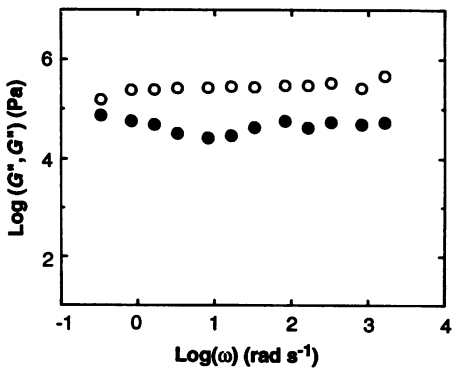

Fig. 4. Log-log plot of storage and loss shear moduli, $G'(\omega)$ and $G''(\omega)$, as a function of angular frequency of measurement, for a film of polymer B of thickness 42 ± 1 Å (3.2 R_G).

and (ii) higher frequencies, where $G'(\omega)$ exceeds $G''(\omega)$. The frequency at the split defines a relaxation time of the system (in this case ~0.1 Hz). This slow relaxation time can be tentatively identified with the kinetics of attachment and reattachment of the adsorbed structures. Qualitatively, the behavior in Fig. 3 resembles the conventional viscoelastic behavior of high molecular weight polymer fluids at the transition between terminal and plateau zones (*13*).

As the films were made thinner, their elastic shear response became stronger and the frequency where $G'(\omega)$ and $G''(\omega)$ split moved to progressively lower frequencies. In Fig. 4, $G'(\omega)$ and $G''(\omega)$ of a film 42 ± 1 Å thick (3.2 R_G) are plotted against ω on logarithmic axes. We note that: (i) the moduli showed minimal dependence on the frequency of deformation, (ii) $G'(\omega)$ exceeded $G''(\omega)$ by nearly an order of magnitude, and (iii) $G'(\omega) \approx 0.3$ MPa. Over the range of film thickness from 30 to 40 Å, changes in $G'(\omega)$ were not detected.

These features would also be typical of a cross-linked or highly entangled rubber in the bulk (*13*). The large strain (~0.1) at onset of a nonlinear response (significantly larger than for a crystal) would also be typical of those systems. Pursuing the analogy, an estimate of the density of effective network strands follows in which the classical equation of rubber-like or entanglement elasticity, $G'(\omega) = (\rho/M_e)(k_BT)$ is used (ρ is the density, M_e is the molecular weight between effective cross-links, k_B is Boltzmann's constant, and T is temperature. The result is that $M_e \approx 6000$ g mol^{-1}. This value is less than the estimated $M_e \approx 12{,}000$ g mol^{-1} in the bulk; the comparison must however be treated with caution in view of the uncertainty in estimating M_e in the bulk. The main point is that M_e in the thin film obviously is larger than the actual size of the molecules.

Another suggestive calculation involves comparing the bulk longitudinal modulus, M (from Fig. 1) and the shear modulus [estimated as $G'(1\text{ Hz})$], to estimate Poisson's ratio (μ) by using standard rheological relations for a continuum system (*13*). Poisson's ratio indicates how much a material contracts when it is extended. When M greatly exceeds the shear modulus, it follows that $\mu = 1/2$ and that no change in volume accompanies the deformation of a material (*13*). The calculations show a monotonic rise from $\mu = 0$ ($P_\perp = 0$) to the limiting value expected of a rubber, $\mu \approx 1/2$ (the thinnest films). This we believe to reflect progressive drainage of unattached chains out of the tethered structures.

What of the dependence on chain length? Experiments with polymer A showed that at $D < 4\ R_G$, $G'(\omega)$ reached the same limiting value as was observed for polymer B at the same film thickness. The generality of the effects described above was thus confirmed.

These are the central experimental results. Let us now restate the problem to be explained. The low compressibility of confined polymer melts has been discussed previously (*1*) but strong shear elastic forces are a qualitatively new phenomenon.

Should one suppose that polymer molecules in this narrow gap actually bridged the two solid surfaces, becoming physically attached to both at once? This structure would produce elasticity in a fashion analogous to the effect of cross-links in a bulk rubber (*22*). Simple calculations suggest, however, that the density of bridging would not be high enough to explain the observed magnitudes of elasticity.

What we believe to be a more likely mechanism comes from an analogy with bulk polymers. Uncross-linked, linear polymers of sufficiently high molecular weight also characteristically exhibit a zone on the frequency scale of relatively slow relaxation, where the magnitude of the elasticity is similar to the levels of G' measured here (*13*). The phenomenon is believed to reflect caging effects, traditionally referred to as entanglements; polymer chains, as they diffuse, can slide by one another but cannot cut across one another, and chain motions become highly correlated (*23, 24*). Similarly, in the system studied here, chains tethered to one surface may be blocked in their motion, over the experimental frequency range, because they cannot cut across other polymer chains that are tethered to the opposing surface. We suggest tentatively that the elastic effects observed here can usefully be viewed as entanglement phenomena—although the chains are too short to be entangled in the bulk.

The motions and relaxations indicated here are thus qualitatively different from those that would characterize the bulk polymer. The frequency-dependent shear forces show the emergence, in these thin films, of a strong elastic component that appeared to reach a limiting value typical of entangled or cross-linked chains in the bulk. The view that entanglement interactions are enhanced in a restricted geometry finds theoretical support (*24*). These observations have evident bearing on understanding a variety of physical situations where conforming surfaces separated by molten polymers come into close contact—especially adhesion, spreading, static friction, and lubrication.

REFERENCES AND NOTES

1. P.-G. de Gennes, in *Liquids at Interfaces: Proceedings of the Les Houches Summer School, Session XLVIII*, J. Charvolin, J. F. Joanny, J. Zinn-Justin, Eds. (Elsevier, Amsterdam, 1990), pp. 296–326.
2. K. Kremer, *J. Phys.* (*Paris*) **47**, 1269 (1986).
3. A. K. Chakraborty, *Macromolecules* **25**, 2470 (1992).
4. P. Silberzan and L. Léger, *ibid.*, p. 1267, and references therein.
5. H. E. Johnson and S. Granick, *Science* **255**, 966 (1992), and references therein.
6. For a review, see D. Ausseré, *J. Phys. France* **50**, 3021 (1989).
7. K. F. Mansfield and D. N. Theodorou, *Macromolecules* **22**, 3143 (1989).
8. R. G. Horn and J. N. Israelachvili, *ibid.* **21**, 2836 (1988).
9. J. P. Montfort and G. Hadziioannou, *J. Chem. Phys.* **88**, 7187 (1988).
10. R. G. Horn, S. J. Hirz, G. Hadziiouannou, C. W. Frank, J. M. Catala, *J. Chem. Phys.* **90**, 6767 (1989).
11. J. N. Israelachvili, S. J. Kott, L. J. Fetters, *J. Polym. Sci. Polym. Phys. Ed.* **27**, 489 (1989).
12. J. Van Alsten and S. Granick, *Macromolecules* **23**, 4856 (1990); S. Granick, *Science* **253**, 1374 (1991).
13. For a review, see J. D. Ferry, *Viscoelastic Properties of Polymers* (Wiley, New York, ed. 3, 1980).
14. M. Denn, *Annu. Rev. Fluid Mech.* **22**, 13 (1990).
15. J. Van Alsten and S. Granick, *Phys. Rev. Lett.* **61**, 2570 (1988).
16. J. Peachey, J. Van Alsten, S. Granick, *Rev. Sci. Instrum.* **62**, 463 (1991).
17. S. J. Clarson, K. Dodgson, J. A. Semlyen, *Polymer* **28**, 189 (1987).
18. S. J. Clarson, J. A. Semlyen, K. Dodgson, *ibid.* **32**, 2823 (1991).
19. J. E. Mark and J. H. Ko, *J. Polym. Sci. Polym. Phys. Ed.* **13**, 2221 (1975).
20. S. M. Aharoni, *Macromolecules* **16**, 1722 (1983).

21. Because of the parallel plate (rather than crossed cylinder) geometry, the Derjaguin approximation commonly used in reporting surface forces measurements (*4–6*) did not apply. For this reason, we report $P_{\perp}$, force normalized by the contact area.
22. J. Klein and P. F. Luckham, *Nature* **308**, 836 (1984).
23. M. Doi and S. F. Edwards, *The Theory of Polymer Dynamics* (Oxford Univ. Press, New York, 1986).
24. J. F. Douglas and J. B. Hubbard, *Macromolecules* **24**, 3163 (1991).

25. We are indebted to J. F. Douglas, J. D. Ferry, G. Reiter, and K. Schweizer for comments and discussions and to S. J. Clarson for donating the PPMS samples used in this study. H.-W.H. acknowledges partial support from grant NSF-MSS-92-02143. We acknowledge primary support of the National Science Foundation through the Materials Research Laboratory at the University of Illinois, grant NSF-DMR-89-20538.

31 July 1992; accepted 5 October 1992

Direct Observation of ClO from Chlorine Nitrate Photolysis

Timothy K. Minton, Christine M. Nelson, Teresa A. Moore, Mitchio Okumura

Chlorine nitrate photolysis has been investigated with the use of a molecular beam technique. Excitation at both 248 and 193 nanometers led to photodissociation by two pathways, $ClONO_2 \rightarrow ClO + NO_2$ and $ClONO_2 \rightarrow Cl + NO_3$, with comparable yields. This experiment provides a direct measurement of the ClO product channel and consequently raises the possibility of an analogous channel in ClO dimer photolysis. Photodissociation of the ClO dimer is a critical step in the catalytic cycle that is presumed to dominate polar stratospheric ozone destruction. A substantial yield of ClO would reduce the efficiency of this cycle.

The mechanisms of polar ozone depletion are well established (*1*). The main catalytic cycle is believed to be (*1*, *2*):

$$ClO + ClO + M \rightarrow ClOOCl + M$$
$$ClOOCl + h\nu \rightarrow ClOO + Cl$$
$$ClOO + M \rightarrow Cl + O_2 + M$$
$$2(Cl + O_3 \rightarrow ClO + O_2)$$
$$\text{Net: } 2O_3 \rightarrow 3O_2$$

The photochemical step in this cycle plays the pivotal role of releasing atomic chlorine from the ClO dimer. This step requires that the Cl–O bond [enthalpy of reaction $\Delta H°(0\ K) = 84$ kJ/mol] breaks preferentially over the weaker O–O bond [$\Delta H°(0\ K) = 67$ kJ/mol] (*3*), and it has been rationalized by the argument that excitation of an $n \rightarrow \sigma^*$ transition localized on the ClO chromophore leads to selective dissociation of the Cl–O bond. In this report, we describe an investigation of the photodissociation of chlorine nitrate ($ClONO_2$) that refutes this argument and thus indirectly raises questions about the photolysis products from ClOOCl.

The notion of selective Cl–O bond fission has evolved from earlier observations that $ClONO_2$ dissociates almost exclusively to Cl and NO_3 (*2*). $ClONO_2$ has been studied extensively because of its importance as a reservoir species for active chlorine and NO_x in the stratosphere (*4*). Earlier studies (*5–11*) reported the dominant channels to be

$$ClONO_2 \rightarrow Cl + NO_3$$
$$ClONO_2 \rightarrow ClONO + O$$

The $\Delta H°(0\ K)$ of these reactions are 167 kJ/mol and 280 kJ/mol respectively. While discrepancies exist in the relative yields for these channels, none of the earlier studies reported dissociation of the weakest bond,

$$ClONO_2 \rightarrow ClO + NO_2$$

which has a $\Delta H°(0\ K)$ of 109 kJ/mol, because the indirect methods used to detect ClO failed to reveal its presence. In an evaluation of data for use in stratospheric modeling, DeMore *et al.* (*12*) preferred the results of Margitan's experiment (*10*), which was a direct study of $ClONO_2$ photolysis at both 266 and 355 nm. With the use of resonance fluorescence to detect Cl atoms and O atoms in a flow cell, Margitan measured Cl and O quantum yields of 0.9 ± 0.1 and 0.1 ± 0.1, respectively. These results have gained broad acceptance.

Although Margitan's experiment lends support to the picture of a transition localized on the ClO chromophore over an argument based on bond energies, the discrepancies among the earlier experiments and their lack of detection of ClO impart uncertainty to the conclusion that the ClO chromophore can be viewed as a distinct entity. Nevertheless, the ultraviolet absorption spectrum (*13*) of $ClONO_2$ shows two overlapping and structureless absorption features that are reminiscent of absorptions in the two chromophores that make up the molecule. The feature with a peak near 215 nm may correspond to an $n \rightarrow \sigma^*$ transition localized on the ClO moiety (*2*), whereas the rise near 190 nm may correspond to a $\pi \rightarrow \pi^*$ transition on the NO_2 group (*14*). Within the confines of this simple picture, each of two wavelengths available with an excimer laser, 248 and 193 nm, should excite one of the respective transitions.

We examined the possibility of bond-selective photolysis of the ClO chromophore in a molecular beam study of the photodissociation of $ClONO_2$ at 248 and 193 nm. With the use of molecular beam methods, we could directly detect the photofragments, identify primary and secondary dissociation channels, and quantitatively determine the relative product yields. We detected both ClO and Cl photoproducts (but not ClONO), and we determined the relative yields of these two products by calibrating the detector sensitivity for ClO and Cl with a Cl_2O photolysis experiment at 308 nm.

Our experiment utilized the technique of photofragment translational energy spectroscopy (*16*) and was performed with a universal crossed molecular beams machine (*17*) in which a pulsed excimer laser beam was substituted for one of the molecular beams (Fig. 1). The laser beam was focused to a spot size of ~0.1 cm^2 where it crossed a molecular beam. The laser fluence was varied over one order of magnitude to check for a power dependence of the various signals observed. Only photoproducts that recoil away from the molecular beam direction can be detected by the mass spectrometer detector, which can be rotated about the molecular beam–laser interaction zone. The distance from the interaction

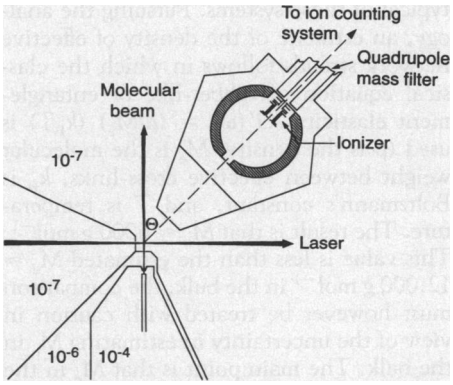

Fig. 1. Schematic diagram of the molecular beam photodissociation experiment. The numbers correspond to pressures in Torr for the various regions. Θ is the detector angle.

T. K. Minton, Jet Propulsion Laboratory, Mail Stop 67-201, California Institute of Technology, 4800 Oak Grove Drive, Pasadena, CA 91109.
C. M. Nelson, T. A. Moore, M. Okumura, Arthur Amos Noyes Laboratory of Chemical Physics, Mail Stop 127-72, California Institute of Technology, Pasadena, CA 91125.